INTERNATIONAL ATOMIC ENERGY AGENCY
UNITED NATIONS EDUCATIONAL, SCIENTIFIC AND CULTURAL ORGANIZATION
INTERNATIONAL CENTRE FOR THEORETICAL PHYSICS
I.C.T.P., P.O. BOX 586, 34100 TRIESTE, ITALY, CABLE: CENTRATOM TRIESTE

H4.SMR/449-17

WINTER COLLEGE ON HIGH RESOLUTION SPECTROSCOPY

(8 January - 2 February 1990)

OPTICALLY PUMPED SUPERSONIC BEAM LASERS: BASIC CONCEPT AND RESULTS

K. Bergmann
U. Gaubatz, H. Bissantz
U. Hefter, I. Colomb de Daunant
P. L. Jones(*)

Universität Kaiserslautern
Fachbereich Physik
Kaiserslautern D6750
F.R. Germany

(*) Dept. of Chem. & Laser Spec. Facility
Ohio State University
Columbus, Ohio 43210, U.S.A.

Optically pumped supersonic beam lasers: basic concept and results

U. Gaubatz, H. Bissantz, U. Hefter,* I. Colomb de Daunant,† and K. Bergmann

Fachbereich Physik der Universität, Postfach 3049, D-6750 Kaiserslautern, Federal Republic of Germany

P. L. Jones‡

Department of Chemistry and Laser Spectroscopy Facility, The Ohio State University, 120 West 18th Avenue, Columbus, Ohio 43210

Received November 28, 1988; accepted February 28, 1989

A comprehensive data set from experiments and model calculations for investigating the behavior of optically pumped supersonic beam lasers is presented. The results for Na_2 demonstrate the roles of stimulated Raman scattering and one-photon population inversion on the gain for collinear optical pumping of supersonic beam gain media for both circular and slit nozzles. For the wavelengths investigated, Raman gain dominates, and an effective photon conversion of greater than 24% is realized. Lasing both with and without frequency-selective elements is studied. Laser transitions terminating on a large range of vibrational levels of the X state are observed. The density-matrix calculations for the gain coefficient include the dynamics of the expansion and the influence of condensation. These results show good qualitative agreement with the experimental data.

1. INTRODUCTION

In this paper we explore the potential of molecular beams as gain media in optically pumped lasers. Studies utilizing optically pumped laser systems play an important role in expanding our understanding of laser behavior, molecular spectroscopy, and chemical kinetics. Optically pumped lasers that operate on a four-level system, such as dye lasers[1] and F-center lasers,[2] are well understood, while the dynamic behavior of an optically pumped three-level system is significantly more complex because of the coherent nature of the process.[3] In the latter the pump field and the Stokes laser field interact simultaneously with the ground and terminal states through the common intermediate level (see Fig. 1). Past work with optically pumped three-level lasers includes studies on the influence of the dynamic Stark effect and Raman processes on laser gain.[3–6] As practical devices optically pumped lasers are interesting for use as line-tunable short-wavelength lasers,[3,4] as local frequency standards,[5] and as high-intensity molecular-beam sources of vibrationally excited molecules.[6,7] Experiments on the population of energetically high-lying vibrational–rotational levels[7] and measurements of collisional-energy-transfer cross sections in cells[8] have also been done. For chemical laser development, demonstration of gain using an optically pumped laser is often an important first feasibility test of the molecular system of interest.[9]

A wide range of three-level optically pumped diatomic lasers is known.[3,9–21] The dimers Na_2 and I_2 have undergone the most extensive investigations as optically pumped gain systems and provide insight into the general features of this class of laser. For example, Wellegehausen and co-workers have demonstrated in Na_2 the origins of the forward–backward gain asymmetry observed for collinear pumping of many dimer-lasing systems.[3] The asymmetry results from stimulated Raman scattering (SRS) contributions to the overall gain.

Compared with that of solid-state or liquid-phase systems, the output power obtainable from these gaseous media is relatively low, because of the small total number of active particles in the relevant molecular states. Nevertheless, output powers up to 200 mW have been observed.[22] In spite of their relatively low output powers the species are high-gain media. Lasing thresholds of the order of a few milliwatts of pump-laser input are achievable from sodium dimer heat-pipe ring lasers with a collinearly pumped gain length of approximately 10 cm, and a gain coefficient of $\lesssim 0.1\ \mathrm{cm}^{-1}$ has been reported.[23]

The quoted results are for experimental configurations that utilize equilibrium cell or heat-pipe arrangements to provide a sufficient density of molecules for laser studies. Although they are experimentally simple to realize, such devices suffer from a number of intrinsic limitations. For example, increasing the maximum usable dimer density is limited as a result of self-absorption and collisional energy losses. For best results in the case of sodium the heat-pipe temperature is maintained within 5% of 800 K, illustrating the delicate dependence on collisional rates, dimer mole fraction, and population distributions necessary to achieve optimum laser performance.[3] Many of these limitations are eliminated through the use of nonequilibrium supersonic expansion molecular-beam sources, as demonstrated through our preliminary work on Na_2 and I_2.[7,14] Strong cooling of the internal degrees of freedom, increased dimer densities, and decreased residence time of the molecules in the cavity owing to the rapid directed flow (see Fig. 2) combine to increase the gain of the system significantly, resulting in some particularly attractive features of this novel laser medium.

In this paper we present a set of experimental results for

0740-3224/89/071386-15$02.00

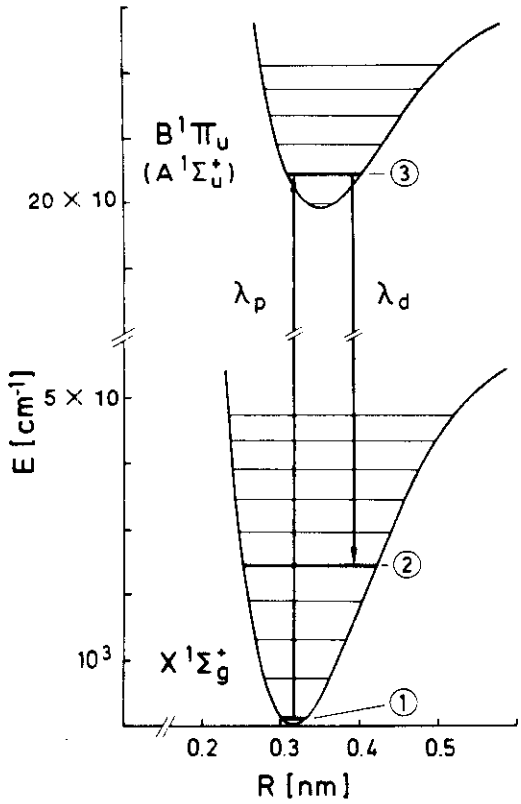

Fig. 1. Potential energy curves and schematic level diagram of the relevant electronic states of the Na_2 molecule.

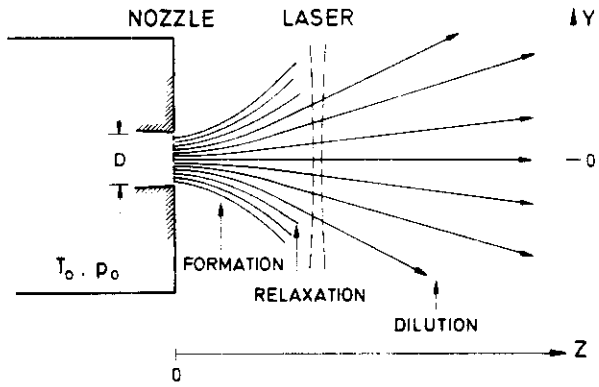

Fig. 2. Flow field in the vicinity of the nozzle. The characteristic regions for dimer formation and relaxations as well as dilution owing to the expansion are indicated. The position of the waist of the laser in the expansion zone is given for $z/D \cong 3$. This distance can be varied by moving the nozzle parallel to the z axis.

the optically pumped Na_2 supersonic molecular-beam laser and examine a comprehensive theoretical model. The analysis explicitly accounts for the behavior of the molecules during supersonic expansions. The gain calculation is done within the framework of existing theoretical models for nonlinear processes. It includes collision processes and Raman gain (see Fig. 3), pump-beam attenuation, and the ac Stark effect. We show that optically pumped supersonic beam lasers may exhibit extremely high gain coefficients. As a consequence, very low threshold pump powers can be expected for lasing. In fact, threshold pump powers below 100 μW have been predicted[12] for optically pumped sodium lasers. So far, they have not been observed in lasers based on heat pipes. However, molecular beams as a gain medium hold promise for achieving threshold pump powers as low as 100 nW. Such devices may become of interest in the effort to develop solar-pumped laser systems.[24] High-gain lasers of this type have also attracted recent interest, because they seem to be ideal systems with which to study dynamical phenomena, such as self-pulsation, period doubling, and chaotic emission.[25,26]

The paper is organized in the following manner: In Section 2 the experimental apparatus is described. Section 3 presents the general characteristics of supersonic beams as gain media. This includes a discussion of the behavior of populations in specific levels $N(v, j)$ for molecules that are formed through condensation during the expansion. Representative experimental results, which examine both inversion and Raman gain, are given in Section 4. In Section 5 the calculation of the gain for optically pumped supersonic beam lasers is presented, and the relevant physical models for the kinetics and optical processes are described. Calculated and experimental results are compared in Section 6. An analysis of the sensitivity of the calculated curves to the assumptions made is included. In Section 7 the work is summarized and the applications of supersonic beam lasers to various areas are considered.

2. EXPERIMENT

A. Overview

The experimental setup is schematically shown in Fig. 4. It consists of a supersonic molecular-beam source, a resonator assembly, and a diagnostics chamber, which is not shown. The vacuum system consists of a source chamber, a differential pumping stage, and a detection chamber used for diagnostic purposes. Sufficient pumping speed is provided to allow molecular-beam operation with carrier gas for enhanced cooling.[27,28] The oven holds approximately 150 g of sodium and operates at temperatures as great as 1025 K, i.e., at vapor pressure of sodium as great as 230 mbars. The nozzle is either a circular hole (0.2–0.5-mm diameter) or a slit (5 mm × 0.03 mm). The beam source used in the experiments is translatable in the x, y, and z directions under vacuum, which permits proper alignment and the variation of the distance between the pump laser and the nozzle.

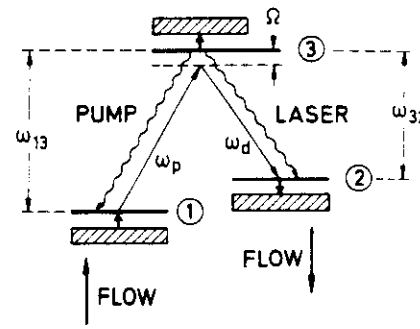

Fig. 3. Diagram of the energy levels 1, 2, and 3 with neighboring reservoir states relevant to the description of the molecular-beam laser. Kinetic couplings are indicated, including the flow of molecules into and out of the cavity, contributing to level population and depopulation. The collisional quenching rate for levels 1, 2, and 3 are γ_1, γ_2, and γ_3, respectively.

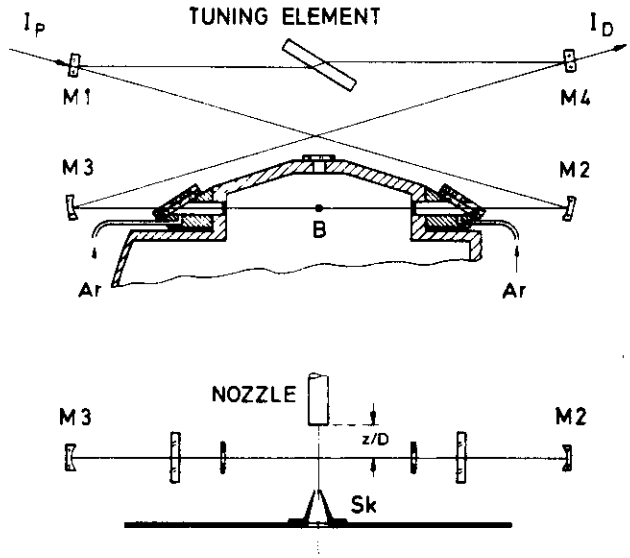

Fig. 4. Experimental setup, showing the ring cavity, formed by the mirrors M1–M4 and built around the molecular beam, B. The tuning element (interference filter or birefringent filter) is used when specific laser transitions (see Fig. 1) are selected. The skimmer, Sk (see the lower part of the figure), separates the region of the nozzle from other vacuum chambers. The Brewster windows (see the upper part of the figure) are heated to prevent sodium deposit. In a more recent setup, a flow of argon, directed toward the windows, is used instead.

The resonator assembly is built around the molecular-beam source in a plane perpendicular to the molecular-beam axis as illustrated in Fig. 4. It consists of a stable four-mirror ring resonator with an interference filter tuning element to select a particular $v' \rightarrow v''$ molecular transition (see Fig. 1). All elements are mounted using thermally compensated mounts on an array of Invar rods that help define the resonator. Two heated Brewster windows sealed with Dupont Kalrez O rings allow the light to be coupled into the vacuum chamber. Heating the windows to 500 K suffices to keep them clear of sodium during source operation. The windows are made from Schott OS glass. A third window is provided as an observation port and can be used for pumping the gain medium perpendicularly with respect to the resonator axis. In a more recent design,[6] we used a flow of argon directed toward the vacuum side of the windows to prevent sodium deposition. This approach is superior to heating but requires a larger pumping speed in order to maintain a sufficiently low background pressure in the vacuum system. After the molecules pass through the resonator, they are trapped in the source chamber (or in subsequent chambers) on cold walls.

B. Optical System

Molecules in the vibrational ground state absorb photons from either an argon-ion laser or a tunable dye laser. In general, the pump laser propagates collinearly to the resonator axis, but a perpendicular arrangement of pump-laser beam and cavity axis is also employed.

The optical resonator is defined by mirrors M1–M4 arranged in a bow-tie configuration (see Fig. 4). The horizontal separation of the mirrors is approximately 390 mm, with a vertical separation of 100 mm. The mirrors M2 and M3 have radii of 353 mm and reflect both the pump-laser and the dimer-laser wavelengths. Mirror M1 and M4 are flats, with M1 having high transmission at the pump-laser wavelength and high reflectivity at the dimer wavelength. The output coupler, M4, typically has a 2% transmission. The mirror M1 is used to couple the pump laser collinearly into the resonator, while M2 is used to focus the pump beam onto the molecular beam. A telescope outside the resonator is used to vary the pump-laser divergence in order to match the waist size of the laser to the cavity mode at the molecular beam. Astigmatism introduced by this resonator design, which uses Brewster windows and spherical mirrors, is partially compensated for by the choice of the incident angle (7.2 deg) of the light onto the mirrors. An analysis of the resonator design shows that an angle of 5 deg would provide full compensation, but this angle is incompatible with the present experimental apparatus.[29]

A transmission interference filter (96% T) having a 4-nm bandpass centered at 540 nm for normal incidence can be inserted into the cavity and can be used to select one vibrational transition for lasing. In a more recent setup[6] laser line selection is accomplished by means of a birefringent filter. No attempt is made to restrict the lasing to a single rotational line, so P- and R-branch transitions are observed simultaneously.

The pump laser for some of these experiments is a single-mode, scannable, and frequency-stabilized argon-ion laser. The 476.5-nm argon-ion line is coincident with the Na_2 $B\,{}^1\Pi_u(v' = 6, j' = 27) \leftarrow X\,{}^1\Sigma_g^+(v'' = 0, j'' = 28)$ transition. The laser can be tuned continuously over its approximately 7-GHz-wide gain profile with a linewidth smaller than the 23-MHz natural linewidth of the Na_2 $B \leftarrow X$ transition. For pumping the sodium dimer on the $A \leftarrow X$ transition, which has a 13-MHz natural linewidth, a tunable dye laser is used in the spectral region 600–650 nm.

3. SUPERSONIC EXPANSIONS AS GAIN MEDIA

A. General Characteristics

The characteristics of supersonic expansions are treated in detail in the literature (see, e.g., Refs. 27–37). In this section the discussion of supersonic expansions is limited to those aspects that are most relevant for understanding the use of the expansions as gain media.

In the region close to the nozzle, the collision frequency in supersonic expansions is high enough to maintain local thermodynamic equilibrium among the translational, rotational, and vibrational degrees of freedom. To a good approximation the process can be considered an adiabatic and isentropic expansion involving an ideal gas. In this case conservation laws for mass, energy, and linear momentum allow one to calculate the variation of density $n(z)$ and temperature $T(z)$ with distance from the nozzle. It is convenient to express these quantities in terms of the Mach number[28,30]

$$M(z) = u(z)/c(z), \tag{1}$$

with $c(z) = (\gamma k_B T(z)/m_t)^{1/2}$. Here γ is the ratio of specific heats, k_B the Boltzmann constant, and m_t the mass per particle. Given the Mach-number function $M(z)$, one can calculate the density and temperature as the expansion develops, using

$$n(z) = n_0 F[M(z)]^{(1/1-\gamma)}, \tag{2a}$$

$$T(z) = T_0 F[M(z)]^{-1}, \tag{2b}$$

with $F(M) = [1 + [(\gamma - 1)/2]M^2]$, while n_0 and T_0 are the density and the temperature, respectively, in the stagnation region of the source. Equations (2) are a reasonable approximation for z less than z_F, the distance to the sudden-freeze surface where thermodynamic equilibrium no longer can be maintained. The value of z_F can be estimated from the stagnation conditions.[28] A detailed description of the beam in the transition region requires a more complex treatment (see, e.g., Ref. 36); however, in the context of this paper, we are interested mainly in the continuum flow region for expansions through both circular and slit nozzles.

For circular nozzles, wind-tunnel measurements of Ashkenas and Sherman[30] combined with theoretical results yield for $z/D > 1$

$$M(z/D) = B(\gamma)\tilde{Z}^{\gamma-1} - [(\gamma + 1)/[2(\gamma - 1)]][B(\gamma)\tilde{Z}]^{(1-\gamma)} + C(\gamma)\tilde{Z}^{-3(\gamma-1)}, \tag{3}$$

where the parameter $\tilde{Z} = (z - z_0)/D$ measures the distance from the nozzle in units of the nozzle diameter. The parameters $B(\gamma)$, $C(\gamma)$, and z_0 are constants that depend on the heat capacity ratio γ of the expanding gas. They are presented in Table 1. At large z Eq. (3) reduces to

$$M(z/D) = B(\gamma)\left(\frac{z - z_0}{D}\right)^{\gamma-1}. \tag{4}$$

The streamline with a distance r^* from the axis at the throat of the nozzle make an angle, θ, with respect to the z axis, given by[31]

$$\tan\theta = g(\gamma)\frac{r^*}{D}B(\gamma)^{1/(\gamma-1)}, \tag{5}$$

with $g(\gamma) = [(\gamma - 1)/(\gamma + 1)]^{(\gamma+1)/[4(\gamma-1)]}$. The angle θ is important in calculating the Doppler profile of the beam for use in the gain calculations of Section 5 below. In the limit of large z all streamlines are straight lines appearing as if they originate at a point z_0 in front of the nozzle.

The range of validity of the measurements of Ashkenas and Sherman is $z/D > 1$. An extrapolation that is valid for $-0.5 < z/D < 1$ and smoothly matches the results of Ashkenas and Sherman at $z/D = 1$, along with the necessary condition that $M(0) = 1$, is[37]

$$M(z/D) = 1.53(z/D + 0.69)^{1.16}. \tag{6}$$

For slit nozzles of width D and length L the Mach function is determined from measurements of Beylich[32] as

$$M(z) = [2[(z/D)^{\gamma-1}/0.53 - 1]/(\gamma - 1)]^{1/2} \qquad z < L, \tag{7a}$$

$$M(z) = [2[(L/D)^{1-\gamma}(z/D)^{2\gamma-2}/0.53 - 1]/(\gamma - 1)]^{1/2} \qquad z > L. \tag{7b}$$

Two distinct regions of the expansion behavior are observed.

Table 1. Parameters of the Mach-Number Function [Eq. (3)] for a Circular Nozzle

Parameter	Atoms	Dimers
γ	5/3	7/5
$B(\gamma)$	3.26	3.65
$C(\gamma)$	0.31	0.20
z_0/D	0.075	0.40

In the near nozzle exit region, parallel streamlines are observed in a plane that includes the long axis of the slit, while a one-dimensional expansion occurs in the direction perpendicular to this plane. In the far-field region, which is of less interest in the context of this paper, the expansion resembles that of a circular nozzle. A good approximation to the Mach-number function for $z \gg L$ is

$$M(z) = [1.94/(\gamma - 1)](L/D)^{-(\gamma-1)/2}(z/D)^{\gamma-1}. \tag{8}$$

When the beam expands into a sufficiently good vacuum, the interaction of the background gas at pressure p_B with the particles of the beam has only a marginal influence on the expansion. For higher p_B the background gas may penetrate into the expansion region, and a shock front develops, which is characterized by a sudden rise in density and temperature.[28] For a circular nozzle, the location of the shock front at the molecular-beam axis is near

$$z_M/D \cong 0.7\left(\frac{p_0}{p_B}\right)^{1/2}, \tag{9a}$$

while, for a slit nozzle, it is found near

$$z_M/D \cong 0.7\left(\frac{p_0}{p_B}\right)^{5/4}. \tag{9b}$$

It is important to realize that a shock develops only if expressions (9) yield $z_M < z_F$, i.e., when the transition to free molecular flow occurs downstream of z_M. When the calculation shows $z_M > z_F$, the densities of the background gas and the beam are too low for strong interaction. The flux of the molecular beam is attenuated, but its thermodynamic properties are not changed significantly.

B. Population Distributions and Condensation Effects

For molecular gases such as I_2 condensation effects are unimportant. However, in alkali supersonic beams condensation of atoms to form dimers during the early phases of the expansion is significant.[34-38] The resulting increase in dimer number density is one of the advantages in using supersonic beams for this work. The nascent molecules are formed in high vibrational levels, and the energy of formation is deposited into the flow as the molecules relax collisionally to low vibrational levels.[34] While it is advantageous for improving the gain of the system, this process complicates the calculation of the temperature characterizing the vibrational and rotational level population.

Dimer formation occurs through a three-body process and is thus restricted to the high-number-density region close to the nozzle. The measurements of Aerts *et al.*[35] indicate that, by $z/D = 0.8$, efficient condensation of atoms to form dimers terminates. The average fraction of dimers at a particular point in the expansion between $0 < z/D < 0.8$ can be described from their work as

$$F(z/D) = F_{oven} + (F_t + F_{oven})G(z/D), \tag{10}$$

with

$$G(z/D) = 2.82 \times 10^{-3} - 0.106(z/D) + 0.356(z/D)^2 - 0.252(z/D)^3 + 0.040(z/D)/[0.310 + z/D].$$

Here F_{oven} is the equilibrium fraction of dimers in the oven at the given temperature and pressure conditions of the source and F_t is the terminal fraction of dimers in the beam. For

Table 2. Parameters Describing the Variation of Temperatures with the Distance from the Nozzle According to Eq. (11)

Degree of Freedom	T_0	T_t	Z_r
Translation	Oven temp.	40 K	2.0
Rotation	Oven temp.	40 K	1.1
Vibration	2000 K	100 K	1.1

sodium, Eq. (10) applies to pressures and nozzle diameters in the range of p_0D between 0.5 and 10 Torr-mm. The expression is assumed valid for p_0D of order 50 Torr-mm, which is the p_0D of our experiment. In this paper an F_t equal to 25% is assumed.

Since the enthalpy of formation adds to the flow in the region up to $z/D = 1$, the temperature development given by Eq. (2b) is replaced for each degree of freedom in Na_2 by the empirical relation

$$T(z) = (T_0 - T_t)\exp(-z/z_r) + T_t, \qquad (11)$$

where T_0 is taken as the oven temperature when the temperature development of rotations and translations is considered but is set to a value of 2000 K in the case of vibrations to account for the effects of condensation. The dependence of the calculated gain on the choice of T_0^{vib} is investigated in Section 5. The terminal temperatures, T_t, are those measured for the source in use, and the scaling parameter z_r is fitted to the experimental results. The values used in Eq. (11) are presented in Table 2. It should be emphasized that the primary uncertainties in our gain calculations for sodium arise from the uncertainties in the concentration of dimers and their vibrational distribution introduced by condensation.

4. EXPERIMENTAL RESULTS

In what follows, Subsections 4.A–4.C as well as 4.F present data obtained without line selectivity of the dimer-laser emission. The data of Subsections 4.D and 4.E have been obtained with an intracavity tuning element.

A. Output Power and Conversion Efficiency

The dimer laser oscillates simultaneously on several transitions with relatively large Franck–Condon factors if no wavelength-selective filter is used in the resonator. Transitions terminating on vibrational levels $5 \le v'' \le 32$ of the Na_2 electronic ground state are observed. Figure 5 presents the variation of the observed dimer laser output power with distance z/D from the nozzle for a range of initial oven temperatures. The variation is typical for a supersonic beam as gain medium when dimer formation occurs in the expansion.

In the early phase of the expansion the heat of formation of dimers delays the cooling process. The population is not sufficiently relaxed to provide a large pool of molecules for optical pumping. The gain is therefore low, and the output power is small. As dimer formation ceases further downstream and relaxation brings the dimers to the lower vibrational levels, the gain rises, as does the observed output power. At larger z/D the streamlines diverge (see Fig. 2), reducing the density of the gain medium and causing the output to drop. The density drops as $(z/D)^{-2}$, but the length of the active medium increases as z/D. Therefore the number of available molecules varies proportional to $(z/D)^{-1}$ and the output power shows a primarily exponential falloff in this region.

As the stagnation pressure increases, the amount of dimer formation increases. The additional heat of formation delays the cooling process to even larger z/D. Consequently the observed maximum of the output power increases and shifts to larger z/D, and the higher dimer density allows lasing to larger values of z/D. Under optimal conditions, when a highly reflective mirror was used as the output coupler ($T < 0.01$) and with efficient cooling by means of a carrier gas, lasing has been observed as far out as $z/D = 100$. This implies for a 300-μm nozzle (see Fig. 6) that the gain is still sufficiently large to support laser oscillation at a distance of 30 mm downstream from the nozzle, which is in the collision-free region of the expansion.

Figure 7 shows the variation of the dimer-laser output power with input pump power for three distances from the nozzle. The results are shown as solid curves. The raw data show fluctuations less than 5%. For $z/D = 1.7$ near the maximum of the output versus z/D, the laser power varies linearly with the pump power up to a value of ~25 mW. At higher pump powers the output power begins to show saturation. As the distance z/D increases, the curves deviate from linearity at lower values of the pump power.

This behavior is consistent with the three-level model described in Section 5. The saturation pump intensity, I_p^0 (see Appendix A), is proportional to the relaxation rates γ_1 and γ_3. The latter decrease with increasing z/D until collisional relaxation ceases, causing the saturation pump intensity to decrease with increasing z/D. In the free-molecular-flow region the relaxation rates become constant and are determined by the flight time through the resonator and, for level 3, additionally by the spontaneous decay rate A_{31}.

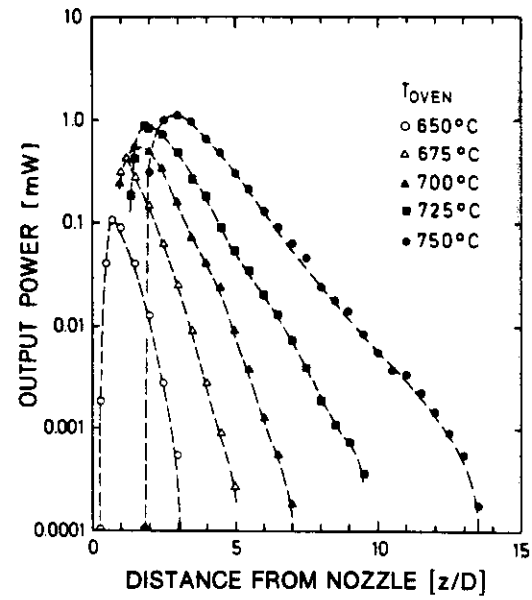

Fig. 5. Variation of the output power with z/D for various stagnation temperatures T_0 in the oven. The nozzle diameter is $D = 500$ μm. The pump-laser wavelength is $\lambda_p = 476.5$ nm. Lasing occurs at several transitions near 500 nm (see Table 3).

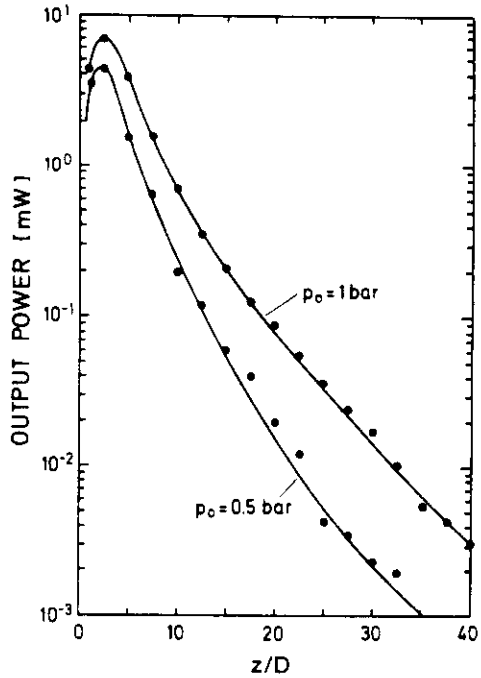

Fig. 6. Variation of the output power with z/D for two different total pressures including the carrier gas argon. The partial pressure of sodium is p_{Na} = 130 mbars. The nozzle diameter is D = 300 μm. The effect of enhanced cooling at higher carrier gas pressure is clearly demonstrated. Pump-laser wavelength is λ_p = 647 nm. Lasing occurred on the $A\,^1\Sigma_u^+$ (v' = 7) → $X\,^1\Sigma_g^+$ (v'' = 5) transition at λ_D = 682 nm.

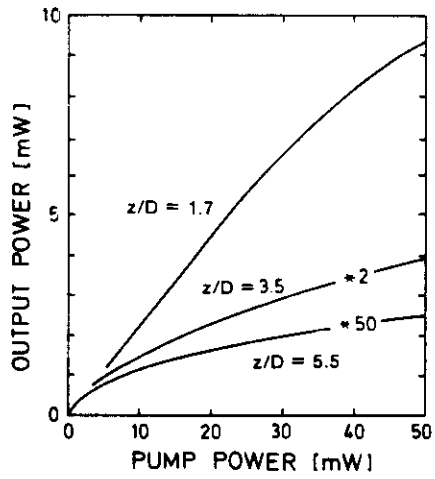

Fig. 7. Variation of the output power with the pump power at various distances z/D downstream of the nozzle. The data for z/D = 3.5 and 5.5 are multiplied by factors of 2 and 50, respectively. The raw data show a fluctuation of less than 5%. Pump-laser and dimer-laser wavelengths are the same as in Fig. 5.

From the slope of the curve for z/D = 1.7 and pump powers less than 25 mW, the efficiency of converting pump power to dimer-laser power is determined to be approximately 25%. Since $\hbar\omega_p > \hbar\omega_D$, the photon conversion efficiency is even larger.

B. Collinear and Transverse Pumping

From the previous results of Wellegehausen[3] it is known that the stimulated Raman process contributes significantly to the gain, with gain due to population inversion between levels 3 and 2 playing only a minor role. The latter contribution to the gain is zero unless the quenching rate γ_2 exceeds the spontaneous decay rate A_{32}. Estimates based on the variation of collisional relaxation with z/D indicate that we typically have $A_{32} > \gamma_2$ for $z/D > 3$. Thus inversion gain is expected to vanish for larger distances from the nozzle.

Direct support of the above from experimental data can be obtained from data taken when the gain medium is pumped perpendicularly to the resonator axis. The large mismatch between the dimer-laser and pump-laser wave vectors that results reduces the Raman gain to a negligible value with respect to the inversion gain, as is shown in Section 5. This allows one to measure the behavior of the dimer-laser output as a function of z/D under conditions dominated by inversion gain. In fact, in pumping the medium transverse to the resonator axis one observes dimer lasing *of equal intensity* in the forward and backward directions. Figure 8 compares the observed variation of the output power for collinear and transverse pumping with z/D under otherwise identical experimental conditions. For transverse pumping lasing terminates at approximately that value of z/D where $A_{32} \cong \gamma_2$.

C. Threshold Pump Power

The variation of the threshold pump power with z/D is of particular interest because of the high gain coefficient for stimulated Raman scattering in this medium. Figure 9 illustrates the pump power required to reach dimer-laser threshold as a function of z/D for three different temperatures. At small z/D the threshold pump power at each temperature is relatively high. The required threshold pump power drops to a minimum value at larger z/D, followed by a plateau region of varying width. At large z/D the threshold rises primarily because of the decrease of particle density in the region of diverging streamlines. Increasing the source temperature decreases the minimum threshold pump power required to produce lasing and shifts the minimum to larger values of z/D. At the same time the width of the plateau region of the curve increases. These results are

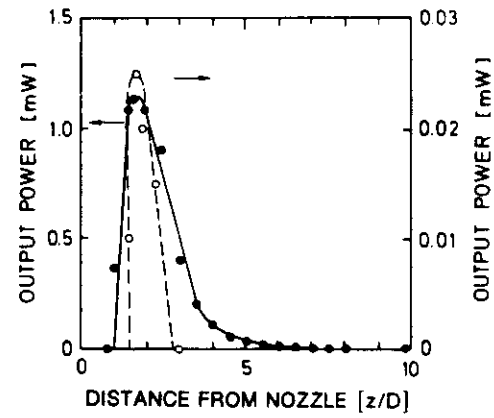

Fig. 8. Variation of the output power with z/D for the standard arrangement of collinear pumping (filled circles, left-hand scale) and for pumping perpendicularly to the axis of the cavity at the location of the molecular beam (open circles, right-hand scale). For the latter arrangement, lasing ceases near z/D = 3 since collisional quenching of the lower laser level is insufficient for maintaining population inversion between levels 3 and 2 (see Figs. 1 and 3). Pump-laser and dimer-laser wavelengths are the same as in Fig. 5.

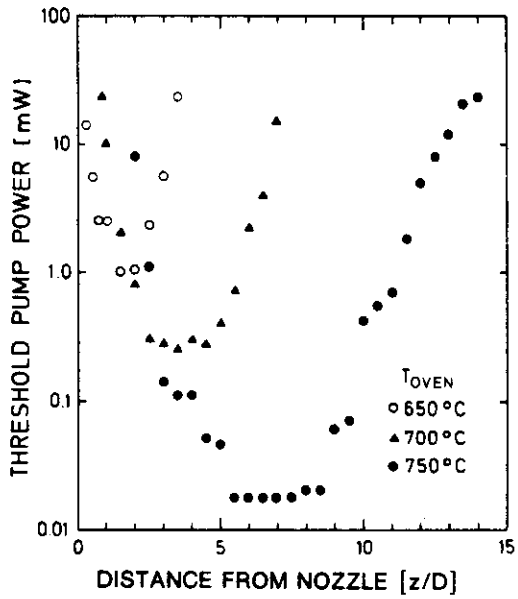

Fig. 9. Variation of the threshold pump power with z/D for various stagnation temperatures T_0 in the oven. Pump-laser and dimer-laser wavelengths are the same as in Fig. 5.

expected because the dimer density, collision rate, and flow velocity increase with increasing source temperature T_0. They are also consistent with the observation that the enhanced dimer formation delays the cooling process owing to the enhanced liberation of heat of formation.

A comparison of these data with the output power curves in Fig. 5 shows that, similar to the trend observed for output powers, higher source temperatures shift the curves to larger z/D. The threshold minimum at a given temperature occurs at a value of z/D consistently larger than that observed for the corresponding output-power maximum. The fact that the locations of the minimum threshold and maximum output do not coincide is not too surprising because they are affected differently by the level populations and pump power. At threshold the system is operated under small-signal conditions, saturation does not occur, and it is highly sensitive to thermal population in level 2. Far above threshold, saturation strongly affects the complex line-shape functions determining the gain, and the output is controlled mainly by the population of level 1.

D. Results with Frequency Selectivity

Introduction of a frequency-selective element such as an interference filter or birefringent filter into the cavity allows the dimer-laser operation to be restricted to a single vibrational transition. This increases the overall cavity losses. In spite of that, lasing is observed to vibrational levels in the range $5 \le v'' \le 32$ for $A \leftarrow X$ pumping. For pumping on the $B \leftarrow X$ transition, lasing occurs for $5 \le v'' \le 15$. By using appropriate pump transitions, lasing in the range $1 < v'' < 40$ is possible. For the latter electronic transition, Fig. 10 shows a roughly linear correlation between the output power and the magnitude of the Franck–Condon factor. The result for $v'' = 5$ falls far off the line. In this case the difference of the wavelength of pump and probe laser is smallest and thus the losses due to increased output coupling are largest. The transitions observed at an oven temperature of 1025 K with a pump power of ~25 mW are presented in Table 3.

E. Expansion with Carrier Gas

Expansion of the alkali vapor in a carrier gas results in more efficient cooling because the condition for continuum flow is maintained up to larger distances z/D. Furthermore, the increased heat capacity of the expanding gas helps to absorb the heat of formation of alkali dimers. As a result, the population in low-lying levels is enhanced, in particular at larger z/D, and a higher output power is to be expected. Figure 6 shows the result for two different total stagnation pressures with argon as a carrier gas. Near the maximum of the curves, the output power increases by a factor of approximately 2 when the stagnation pressure is raised from $p_0 = 0.5$ bar to $p_0 = 1$ bar. Further downstream the increase is as large as a factor of 5. Of course, when a noncondensable

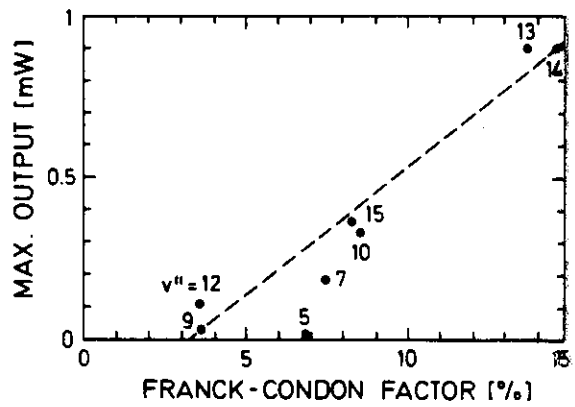

Fig. 10. Maximum output power for transitions to several vibrational levels v'' plotted versus the relevant Franck–Condon factors. The pump power at $\lambda_p = 476.5$ nm was 25 mW. The transmission of the output coupler was 2%. The data were taken at the stagnation conditions $p_0 = 130$ mbars, $T_0 = 975$ K.

Table 3. Observed Transitions for Frequency-Selected Operation of the Na_2 Laser

Pump-Laser Transition λ_p (nm)	Laser Wavelength λ_D (nm)	Lower Laser Level v''	FCF[a] (%)
$B\,^1\Pi_u \leftarrow X\,^1\Sigma_g^+$	531.9	15	7.8
$v' = 6 \leftarrow v'' = 0$	528.1	14	14.3
$\lambda_p = 476.5$ nm	524.3	13	14.2
FCF = 5.9%	520.5	12	9.4
	513.0	10	8.2
	509.2	9	4.5
	501.8	7	7.6
	494.4	5	4.5
$A\,^1\Sigma_u^+ X \leftarrow X\,^1\Sigma_g^+$	801.6	21	3.9
$v' = 7 \leftarrow v'' = 0$	793.6	20	4.9
$\lambda_p = 646.8$ nm	785.7	19	13.9
FCF = 11.2%	762.1	16	6.9
	739.2	13	5.4
	716.8	10	4.8
	680.9	5	5.1
	667.0	3	4.3
$A\,^1\Sigma_u^+ \leftarrow X^1\Sigma_g^+$	812.5	32	120
$v' = 17 \leftarrow v'' = 0$	805.7	31	2.7
$\lambda_p = 604.4$ nm	798.9	30	1.4
FCF = 1.0%			

[a] Franck–Condon factor.[50]

carrier gas is used, a significantly larger pumping speed is required.

F. Preliminary Results for Slit Nozzles

In the context of this work, it is a disadvantage to use an expansion through a circular nozzle since the effective active length of the gain medium is then quite short. An angle of 1 deg of the flight path of a molecule relative to the molecular beam axis results in a mean Doppler shift of ~35 MHz, which is larger than the natural linewidth of the molecular transition. Because the distance along the streamline and the angle are small, the usable length in the direction of the laser propagation is also small. Figure 11 shows the variation of output power and threshold pump power with the vapor pressure in the oven for a fixed distance from the source and the $B(6, 27) \leftarrow X(0, 28)$ transition. The output power increases approximately linearly with increasing p_0, while the threshold pump power decreases exponentially. It is tempting to extrapolate these data to even higher p_0 and to temperatures greater than $T_0 > 750$°C. However, the material consumption then becomes excessively high, which limits one's enthusiasm for attempting the measurements.

By providing a near-parallel flow field, slit nozzles offer an opportunity to increase significantly the effective length of the gain region. In a preliminary experiment we replaced the circular nozzle by a slit of equal area having dimensions of $L = 5$ mm and $D = 0.03$ mm.

Figure 12 shows representative results for the variation of the dimer-laser output and the pump power required to reach dimer-laser threshold at a source temperature of 975 K. The data are for pumping the $B(6, 27) \leftarrow X(0, 28)$ transition. The maximum output power is higher for the slit nozzle than for the circular nozzle as expected because of the increased length of gain medium in the former case. The observed threshold is lower as well for the same reasons.

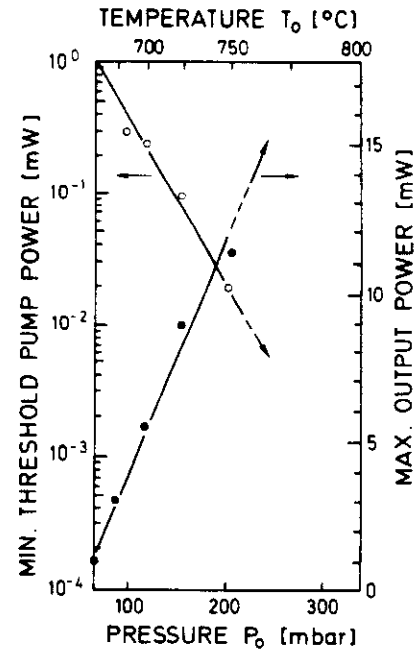

Fig. 11. Variation of output power (filled circles, left-hand scale) and threshold pump power (open circles, right-hand scale) with the vapor pressure p_0 in the stagnation region. These data are taken for $\lambda_p = 476.5$ nm and multiline laser operation.

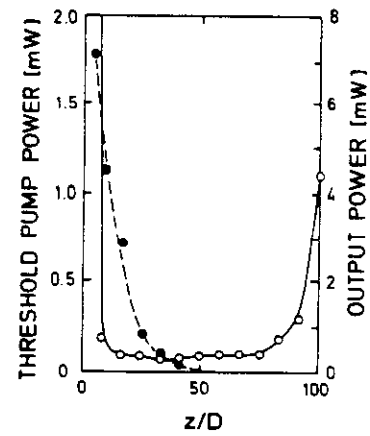

Fig. 12. Variation of the output power (filled circles, right-hand scale) and threshold pump power (open circles, left-hand scale) for the $B(6, 27) \rightarrow X(0, 28)$ transition with the distance from the nozzle for a slit nozzle of width $D = 0.03$ mm and length $L = 5$ mm. The source temperature is $T = 975$ K. Pump-laser and dimer-laser wavelength are the same as in Fig. 5.

5. GAIN CALCULATIONS

A. Derivation of the Gain Coefficient

The gain coefficient $\alpha_D = -(1/I_D)(dI_D/dz)$ is the basic quantity that must be determined for the calculation of the output power and the threshold pump power of the dimer-laser system. It is given by[3]

$$\alpha_D = -k_D \operatorname{Im}(2\hbar c \rho_{23} V_D / I_D) \tag{12}$$

and is related to the nondiagonal element ρ_{23} of the density matrix. The Rabi frequency $V_D = 0.5 p_{23} E_D/\hbar$ represents the coupling between levels 2 and 3. The transition dipole moment, the electric field, the intensity, and the wave number of the dimer laser are p_{23}, E_D, I_D, and k_D, respectively.

The calculation of the gain, based on a density-matrix approach,[3,39–43] uses the kinetic scheme illustrated in Fig. 3. The detunings of the pump and dimer lasers from resonance with the molecular transitions ω_{ik} are given by $\Omega_p = \omega_p - \omega_{31}$ and $\Omega_D = \omega_D - \omega_{32}$, respectively. For simplicity the molecular energy levels are reduced to a three-level system, each level of which is coupled to a reservoir formed from all remaining levels. Collisional transfer into the reservoirs is possible at rates γ_{1C}, γ_{2C}, and γ_{3C}. The reverse process is negligible for levels 2 and 3 since the neighboring levels are virtually unpopulated for $z/D > 1.5$. Spontaneous emission out of level 3 to level 1 or 2 is possible with rates A_{31} and A_{32}, which depend on the Franck–Condon factors for the transitions involved. The inverse of the spontaneous radiative lifetime of level 3 is A_3. For the homonuclear molecules under consideration there is no radiative coupling by one-photon transitions between levels 1 and 2.

The total relaxation rates of level i, γ_i, include spontaneous emission and all nonradiative processes such as collisions γ_{ic}. The rapid directed flow (1500 m/sec) also leads to a relaxation process because the molecules leave the resonator quickly and appear as a loss to the gain medium. This relaxation mechanism (time-of-flight relaxation) allows suf-

ficient Raman gain to permit cw dimer-laser action in the region of free molecular flow.

The relaxation rates γ_{ij} describe the damping of the off-diagonal elements of the density matrix ρ_{ij}, i.e., the polarization of the medium for the respective transitions. Normally, they exceed the γ_i because of phase-changing collisions and thus obey the rule[44] $\gamma_{ij} \geq \frac{1}{2}(\gamma_i + \gamma_j)$. In the collision-free region of a molecular beam the equality sign applies.

Within the rotating wave and steady-state approximations,[40] and when a classical treatment of the electromagnetic fields of standard form is used, the differential equations describing the evolution of the density matrix needed for this problem reduce to a set of algebraic equations[3] that can be solved by standard methods. Analytical solutions for the gain coefficients $\alpha_p{}^v$ and $\alpha_D{}^v$ for the pump and dimer laser radiation, respectively, are given in Appendix A.

In the case of low dimer-laser power I_D, the gain coefficient $\alpha_D{}^v$ can be expanded in a series in I_D and the lowest-order contribution yields three terms that are easy to interpret:

$$\alpha_D{}^v = \sigma_D\left\{\rho_{22}{}^0 E(v) - \rho_{11}{}^0 \frac{\gamma_1}{\gamma_1+\gamma_3}\frac{P}{1+P} \times\left[(1 - A_{32}/\gamma_2)\delta_{13}{}^P(v)E(v) + \frac{\gamma_3}{2\gamma_{13}}G(v)\right]\right\}. \quad (13)$$

The derivation of this formula[3,43] is briefly described in Appendix A. The absorption cross section for the dimer-laser transition is $\sigma_D = k_D|p_{32}|^2/(\epsilon_0\hbar\gamma_{23})$. The variables $\rho_{11}{}^0$ and $\rho_{22}{}^0$ are the equilibrium-level populations without any fields. In a molecular-beam environment $\rho_{22}{}^0$ can normally be set to zero.

The pump parameter P is proportional to the pump-laser field E_p and indicates the degree of saturation for that transition; specifically, P is the ratio of the pump-laser Rabi frequency, $V_p = p_{13}E_p/(2\hbar)$, and the factor $\gamma = 0.5\gamma_{13}\gamma_1\gamma_3/2(\gamma_1 + \gamma_3)$ involving relaxation rates. The line-shape functions $E(v)$, $\delta_{13}{}^P(v)$, and $G(v)$ depend on the relaxation rates, the pump parameter P, the detunings of the laser frequencies $\Omega_P = \omega_p - \omega_{13}$ and $\Omega_D = \omega_D - \omega_{23}$, and the velocity v of the molecules through the Doppler shifts $k_{P,D}v$. The explicit form of these functions is given in Appendix A [Eqs. (A6)–(A8)].

The first term of Eq. (13) represents the self-absorption of the dimer laser that is due to an initial population $\rho_{22}{}^0$ in level 2. For small pump-laser power P its frequency dependence reduces to a Lorentzian line shape of width γ_{23}. This term is negligible for vibrational levels $v'' > 0$ in a molecular-beam environment since $\rho_{22}{}^0$ is effectively zero. The second term can be identified as the gain arising because of an inversion between levels 3 and 2. It contains the factor $(1 - A_{32}/\gamma_2)$, which changes sign when the relaxation rate γ_2 drops below the spontaneous emission rate A_{32}. It is responsible for limiting lasing to small z/D in the transverse pumping arrangement. The product $\rho_{11}{}^0\{P/(1 + P)\}\delta_{13}{}^P$ in this term gives the number of molecules that are transferred by the pump laser to level 3, with $\delta_{13}{}^P(v)$ being a power-broadened Lorentzian line-shape function for the pump-laser transition. The third term is characteristic for a three-level laser system. It represents the gain due to the Raman process.

Usually, under the conditions of our experiment, the first two terms of Eq. (13) are unimportant. Therefore the behavior of the third term, the Raman gain, is of particular interest. Thus it is necessary to examine the behavior of the function $G(v)$ in greater detail. Here v is the component of the molecular velocity parallel to the axes of the laser beams. The function $G(v)$, appropriate for this process, is shown in Fig. 13 as a function of the velocity v or the normalized Doppler shift k_Dv/γ_{13} for both copropagating and counterpropagating laser fields. It reaches a maximum when the resonance condition

$$(\Omega_p - \Omega_D) - (k_p - \epsilon k_D)v = 0 \quad (14)$$

is obeyed; this is just the condition for energy conservation in a system in which Doppler-shift energy compensation is possible. The directional asymmetry of the line shape is clearly revealed.

When Ω_D and Ω_p are fixed, energy conservation yields a unique velocity component, v_{res}, for which it is satisfied. However, the finite linewidth of the two-photon transition $\Delta\omega_{12}$ brings molecules in the velocity range Δv near the velocity v_{res} into resonance with the laser fields, according to Eq. (14). This velocity range is given by[3]

$$|k_p\Delta v| = \Delta\omega_{12}/(\epsilon k_D/k_p - 1). \quad (15)$$

It is smaller for counterpropagating fields ($\epsilon < 0$) than for copropagating ones, resulting in a smaller gain for the former as opposed to the latter. Moreover, for counterpropagating fields absorption occurs for molecules with velocity components farther away from v_{res}. Experimentally this reveals itself as a forward–backward asymmetry in the output power of the dimer laser. In fact, for Na_2-beam lasers no emission is seen in the propagation direction opposite that of the pump laser.[14] In I_2 a forward-to-backward intensity asymmetry of 10 to 1 is observed.[7]

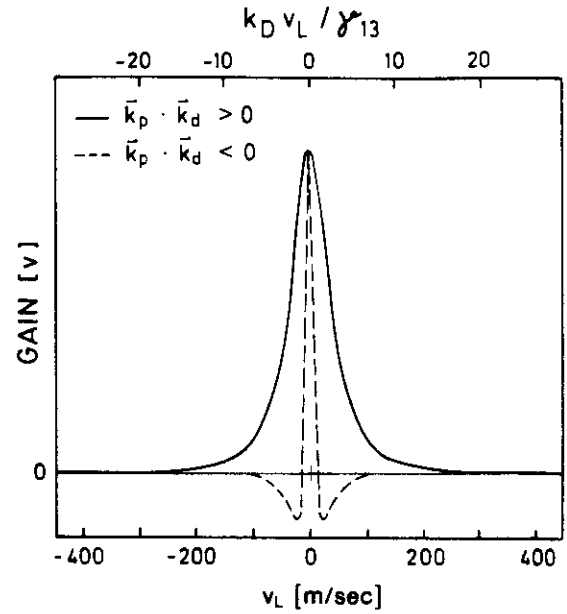

Fig. 13. Variation of the gain with the velocity component v_L in the direction of the laser beam for copropagating (solid curve) and counterpropagating (dashed curve) pump and laser beams. The scale on the top gives the dimer-laser frequency detuning in units of the linewidth of the pump transition.

B. Velocity-Integrated Gain

A molecule contributes to the net gain α_D of the dimer laser, according to its velocity component v. The corresponding distribution function is $f(v)$. Assuming for $f(v)$ a Maxwell distribution of width $(2k_BT/m_I)^{1/2}$, which is much broader than the line-shape functions $\delta_{13}{}^P(v)$, $E(v)$, and $G(v)$, the velocity integrations can be performed analytically in the limit of small pump-laser intensity I_P.[3,4] It can be shown[42] that, in the limit of low pump-laser and dimer-laser fields, the velocity-integrated contribution $G(v)$ of the two-photon transition to the gain is zero for $\epsilon < 0$.

C. Output Power and Threshold Calculations

The output power and the threshold pump power have been calculated numerically without any approximations to the gain concerning low pump- or dimer-laser power. The steady-state gain coefficient is also given in Appendix A [see Eq. (A4)]. It depends on the detunings, which obey the two-photon resonance condition, Eq. (14). The other variables are local parameters that vary with the location of the pump laser in the amplifying medium. They are calculated based on the modeling of the expansion as discussed in Section 3. The total gain coefficient results, therefore, from the gain coefficient at first integrated over the velocity distribution at each position of the beam and then integrated along the amplifying medium. The latter integration has been simplified by a one-dimensional summation over the propagation direction of the laser fields while taking into account the decrease of the pump-laser intensity as it propagates through the medium. Thus the intensities of the electromagnetic fields are considered constant transverse to their propagation directions up to a distance $\pm w_0/2$ from the beam center, with w_0 being the beam waist size. Here w_0 is 75 μm for both beams. This also implies that variation of the population of the molecular levels with y is ignored. Although these assumptions may lead to an overestimation of the calculated gain, they considerably reduce the computation time without affecting the qualitative value of the results. In addition, a number of other approximations of less consequence have been made:

(i) The dimer-laser field is not treated as a dynamical variable but is taken as a parameter for these calculations. Thus Maxwell equations that correlate the variation of the Stokes field with the polarization of the medium induced by the laser fields[45] are not included in the computational process.

(ii) The number density on the molecular-beam axis and the streamlines of the expansion are assumed to be given by the Mach-number function.

(iii) The streamlines of the expansion are assumed to be straight lines starting at the nozzle and are thus defining the mean Doppler shift for the fields.

(iv) The angular distribution of the beam flux varies[31] according to $\cos^3\theta$.

(v) The collisional relaxation rates are estimates.

(vi) The integration limits are given by the most probable velocity of the Lorentzian velocity distribution and the $1/e$-width of the laser fields. The length of the amplifying medium is limited by those streamlines that start near $z = 0$ at a distance $r = D/2$ from the axis.

The actual gain calculation proceeds as follows: For given z, the Mach-number function $M(z)$ and the parameters describing the supersonic beam are determined according to Eq. (3) or (7) and Eqs. (10) and (11), respectively. The gain is calculated by propagating the laser beams across the gain medium in small steps, employing Eqs. (A3) and (A4) of Appendix A. For threshold calculations the initial dimer-laser intensity is set to zero. At each step in the y direction, the local density level, populations, collision rates, and the angle between the streamline and the field, giving the mean local Doppler shift, are determined. The absorption coefficient or gain coefficient for the pump or dimer laser, respectively, is then integrated over the velocity distribution at this value of y. The decrease of the pump field intensity is determined, and the dimer-laser gain coefficient is stored. This procedure is repeated until the fields have propagated through the medium.

In the steady-state limit the dimer-laser intensity is considered constant and is determined by the value of the gain coefficient resulting from integration over the length of the active medium. This value is labeled $G(I_D)$. The overall dimer intensity in the resonator is implicitly given by the conditions[46]

$$C^{1/2}\exp[G(I_D) - L] = 1,$$

where C and L are the transmission efficiency and the losses in the cavity, respectively. This condition is valid for steady-state operation, where the overall gain and loss balance. The calculated output of the dimer laser is $0.02I_D$. The calculated results are compared with experimental data in Section 6.

6. CALCULATED RESULTS AND COMPARISON WITH EXPERIMENTAL DATA

In Fig. 14 the calculated variations of output and threshold with the distance z/D from the nozzle are compared with experimental data at 975 and 1025 K. The input parameters for the calculations are given in Tables 1 and 2. The collision cross sections are taken as $\sigma_1 = 100$ Å^2, $\sigma_2 = 300$ Å^2, and $\sigma_3 = 500$ Å^2. The cross sections are estimated because measured values are available only for room temperature. Here, the collision rates at the very low temperature prevailing in the expansion zone are relevant and may vary significantly with the vibrational level.[47] The resonator losses are estimated to be 7% (including 2% from the output coupler M4 and filter losses of 4% to achieve single-frequency lasing). As expected, the absolute values of the calculated output and threshold pump power agree with the experimental results only within an order of magnitude.

The accuracy of the calculated data suffers mostly from the difficulty in determining the absolute number densities for ground-state-level populations and from the other assumptions made in the model. The variation of output and threshold pump power is, however, reproduced well within the experimental error. Also, the shift of the maximal output power and the minimal threshold power as a function of z/D is confirmed by the numerical calculations.

The observed and calculated variation of the dimer laser output power with input pump laser power is shown in Fig. 15. The theoretical curve reaches saturation at lower pump-laser powers than the experimental curves. This is consis-

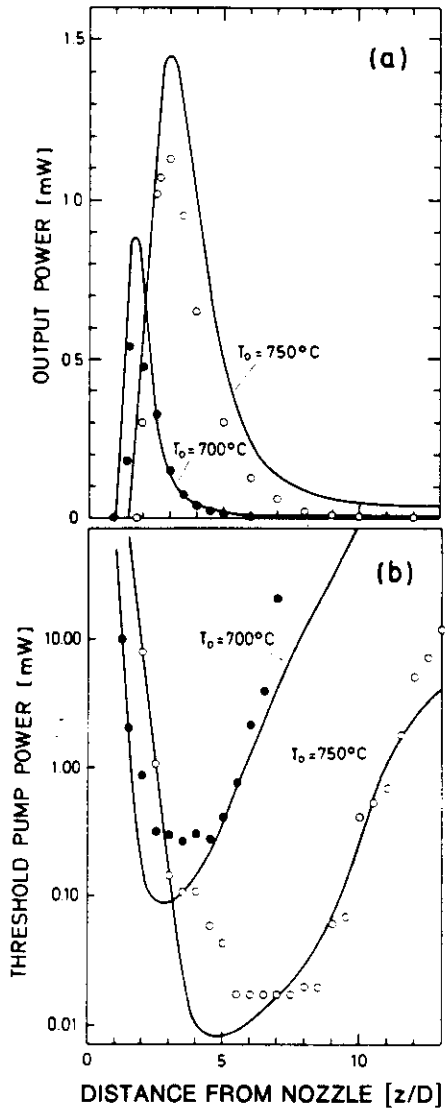

Fig. 14. Comparison of the calculated (solid curves) and measured variation of (a) output power and (b) threshold pump power with z/D. The relevant temperatures in the expansion zone are modeled according to Eq. (11) with the parameters given in Table 2. Pump-laser and dimer-laser wavelength are the same as in Fig. 5.

tent with the expectation that the collision rates at the low temperatures prevailing in the beam are larger than at room temperature, since the saturation intensity depends linearly on the relaxation rates γ_1 and γ_3. The lack of sufficiently accurate data about collision processes at low temperatures, which govern the saturation behavior, prohibits a more detailed analysis at this time.

The observed variation of the output power with z/D is shown for three terminal laser levels v'' in Fig. 16(a). In Figure 16(b) the variation of the calculated gain in the small-signal limit ($I_D = 0$) is shown. The output power was not calculated because the information about the overall loss was insufficient in this case. As expected, the maximum gain is found for positions z/D downstream of the maximum output power. In fact, for $v'' = 7, 10, 14$, the lowest threshold pump power is observed in the range $3 \leq z/D \leq 4$. Tests of the sensitivity of the theoretical curves to the choice of input parameters can be made to assess the reasonableness of the parameter values chosen and to provide insight into the influence of various parameters on the laser performance. Results are shown in Fig. 17. The vibrational temperature [see Eq. (11)] is enclosed in quotation marks because it is essentially a parameter that describes the ratio of the population of levels $v'' = 0$ and $v'' \gg 1$. The rapid

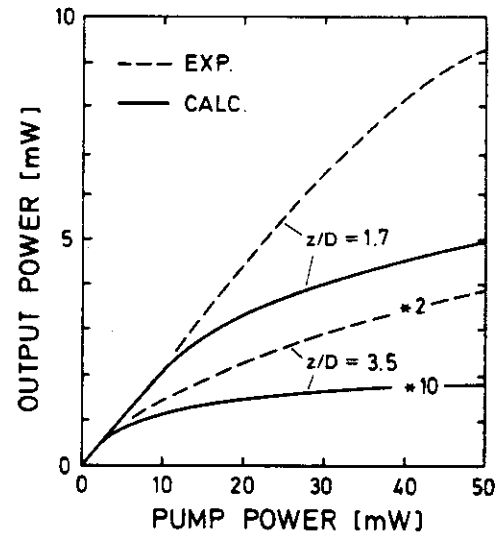

Fig. 15. Comparison of calculated (solid curves) and measured (dashed curves) variation of the output power with pump power for two different positions z/D downstream of the nozzle. The experimental and calculated data for $z/D = 3.5$ have been multiplied by factors of 2 and 10, respectively.

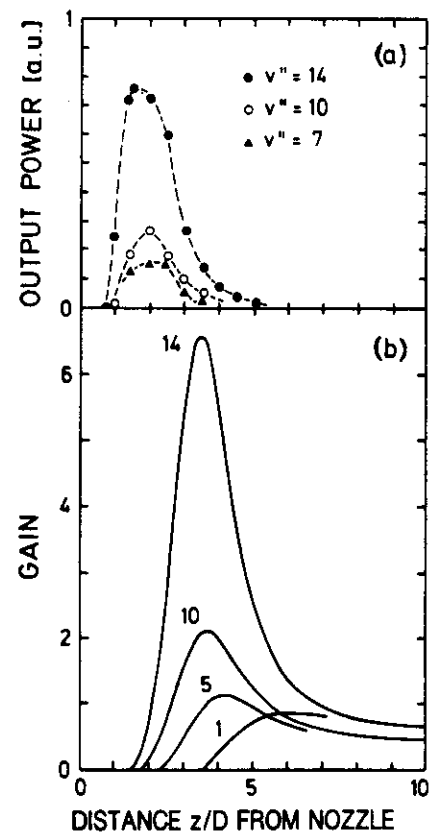

Fig. 16. Variation of (a) the observed output power and (b) the calculated gain with the distance z/D from the nozzle for transitions to selected vibrational levels v''. The transitions between the electronic B and X state are specified in Table 3.

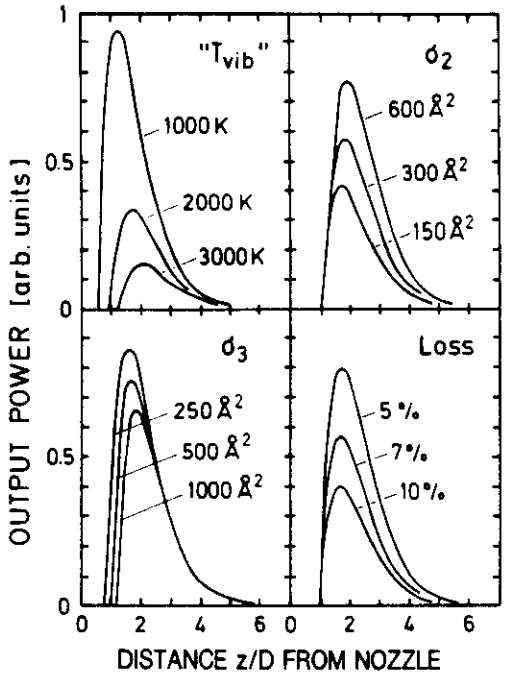

Fig. 17. Variation of the calculated output power with the distance z/D from the nozzle, showing the sensitivity to the initial vibrational temperature [see Eq. (11)], the collision cross sections σ_2 and σ_3 for levels 2 and 3, respectively, and the total loss of the cavity.

decrease of the output power with increasing T_{vib} results mainly from a decrease in the number of molecules in level 1 at small z/D, where the densities are the highest. The cross section σ_2 for the depopulation of level 2 and the polarizations ρ_{12} and ρ_{23} affect the maximum output power but have little effect in the threshold region. Collisional losses of level 3 do affect the laser performance in the region near the nozzle but not at larger z/D. This is because the relaxation of level 3 is dominated by spontaneous emission at large distances from the nozzle. The variation of output power with cavity loss L is also shown in Fig. 17. For $5\% \leq L \leq 10\%$ the threshold is reached at nearly the same distance from the nozzle in each case. Figure 17 demonstrates that the popu lation of level 1 is the most relevant one to use in determining output and threshold pump power behavior and that the cooling process of the internal degrees of freedom dominates the laser performance in the region $1 \lesssim z/D \lesssim 2$.

7. SUMMARY AND CONCLUSIONS

We have discussed some unique features of supersonic beams as a gain medium for optically pumped lasers. These systems exhibit extremely large gain coefficients and provide significant advantages over conventional cells and heat pipes as sources for gain media. The results of our experiments confirm conclusively that the high gain observed in the Na_2-beam laser is a result of stimulated Raman scattering contributions. The variations of calculated output and threshold pump power with the distance from the nozzle agree well with the experimental results. The absolute magnitude is, however, not reliably reproduced because of the lack of sufficiently accurate data about number densities, collision processes, and dimer formation in the expansion zone. Further significant improvement of performance is expected from scaling the use of slit nozzles to increase the length of the gain medium.

The unique nature of this type of laser system is permitting new applications for optically pumped lasers in scientific research. For example, we have recently investigated the application of this system as an intense source of vibrationally state-selected molecules for use in scattering and energy-transfer experiments.[6] Additionally, because of the observed low threshold pump power, this system holds promise as a candidate for solar pumping in spite of the coherent nature of the conversion process of pump photons to laser photons. Furthermore, in the area of fundamental laser physics, investigations of the role of pump-laser photon fluctuations on optically pumped lasers in a ring cavity[48] can be made. Finally, we may speculate on the use of this laser as an amplifier for laser radiation at a specific wavelength in the blue and red regions of the spectrum. In particular, this will be interesting if the slit nozzles can be scaled to even larger lengths.

The use of molecular beams as sources for optically pumped lasers is not restricted to Na_2. Lasing has been observed within I_2 beams[7,49] and K_2 beams as gain media. Using other molecules, such as NO, as the gain medium holds promise for laser lines offering broad tunability in the UV spectral region.

APPENDIX A

For completeness we summarize the relevant formulas here, as they have been used in the numerical relations.

Basic Equations

The derivation of Eq. (13) is based on the Schrödinger equation in the density-matrix formalism:

$$d\rho/dt = -i/\hbar(H\rho - \rho H) - \rho_{rel} + \rho_s, \tag{A1}$$

where ρ is the density matrix that describes the temporal evolution of the system under the action of the Hamiltonian H; ρ_{rel} is a relaxation matrix coupling the molecular levels of interest to the reservoir, formed by all other levels; and ρ_s is a spontaneous decay matrix. The relaxation matrix ρ_{rel} has the following form:

$$\rho_{rel} = \begin{bmatrix} \gamma_1(\rho_{11} - \rho_{11}^0) & \gamma_{12}\rho_{12} & \gamma_{13}\rho_{13} \\ \gamma_{12}\rho_{21} & \gamma_2(\rho_{22} - \rho_{22}^0) & \gamma_{23}\rho_{23} \\ \gamma_{13}\rho_{13} & \gamma_{23}\rho_{32} & \gamma_3\rho_{33} \end{bmatrix}. \tag{A2}$$

Thermal populations are given by ρ_{ii}^0. The γ_i and γ_{ij} are described in Subsection 5A; the relaxation rate γ_3 also contains the spontaneous emission rate A_3. The coupling of the levels 1, 2, and 3, because of spontaneous decay, is given by the matrix elements $\rho_{s,11} = A_{31}\rho_{33}$ and $\rho_{s,22} = A_{32}\rho_{33}$.

H includes the Hamiltonian H_0 for the unperturbed molecular system with eigenvalues $\hbar\omega_{ij}$ and the dipole operator, pE. The matrix p contains the dipole moments for the respective transitions. The electric field E has the following form:

$$E = (E_p/2)\exp[-i(\omega_p t - k_p y)] + (E_D/2)\exp[-i(\omega_D t - \epsilon k_D y)] + \text{c.c.}$$

The parameter $\epsilon = \pm 1$ defines the propagation direction of the dimer laser E_D relative to the pump laser E_p. As usual

the rotating wave approximation and the slowly varying envelope approximation[3,45,46] are applied to solve Eq. (A1). Since the motion of the molecules is relevant, the time derivative d/dt is given explicitly by $\delta/\delta t + v\,\delta/\delta y$, where v is the velocity of the molecules along the laser propagation direction. When this form is used, the dependence of the density matrix in the x and z directions is neglected. Under steady-state conditions Eq. (A1) reduces to an algebraic system of nine equations that can be solved for the imaginary part of ρ_{ij}. The latter is related to the gain of the corresponding transition through Eq. (12).

General Solutions

The general solutions for the gain coefficients are[3]

$$\alpha_p{}^v = \sigma_p\gamma_{13}/N_0[-A\rho_{11}{}^0 + B\rho_{22}{}^0 - 2(AC - BD)|V_D|^2 \times (\Gamma_{23}\rho_{11}{}^0 - \rho_{22}{}^0(1 - A_{31}/\gamma_1)/\gamma_3)] \quad \text{(A3)}$$

and

$$\alpha_D{}^v = \sigma_D\gamma_{23}/N_0[C\rho_{22}{}^0 - D\rho_{11}{}^0 + 2(AC - BD)|V_p|^2 \times (\rho_{11}{}^0(1 - A_{32}/\gamma_2)/\gamma_3 - \rho_{22}{}^0\Gamma_{13})], \quad \text{(A4)}$$

with

$$\Gamma_{13} = (\gamma_1 + \gamma_3)/(\gamma_1\gamma_3), \qquad \Gamma_{23} = (\gamma_2 + \gamma_3)/(\gamma_2\gamma_3)$$

and the Rabi frequencies

$$V_p = p_{13}E_p/(2\hbar), \qquad V_D = p_{23}E_D/(2\hbar).$$

Furthermore,

$$A = \mathrm{Im}[(\Delta_{23}{}^*\Delta_{12} + |V_p|^2)/N],$$

$$B = \mathrm{Im}[|V_D|^2/N],$$

$$C = \mathrm{Im}[(|V_D|^2 - \Delta_{13}{}^*\Delta_{12}{}^*)/N^*],$$

$$D = \mathrm{Im}(|V_p|^2/N^*).$$

The asterisks indicate complex-conjugate values. The complex frequencies depend on the molecular velocity v, the relaxation rates γ_{ij}, and the frequencies ω_p, ω_D, and ω_{ij} according to

$$\Delta_{13} = -\Omega_p + k_pv + i\gamma_{13},$$

$$\Delta_{23} = -\Omega_D + \epsilon k_Dv + i\gamma_{23},$$

$$\Delta_{12} = (-\Omega_P + k_Pv) + (\Omega_D - \epsilon k_Dv) + i\gamma_{12},$$

with

$$\Omega_p = \omega_p - \omega_{13},$$

$$\Omega_D = \omega_D - \omega_{23}.$$

N is given by

$$N = \Delta_{12}\Delta_{13}\Delta_{23}{}^* + \Delta_{13}|V_p|^2 - \Delta_{23}{}^*|V_D|^2,$$

while we have

$$N_0 = 1 + 2|V_D|^2(C\Gamma_{23} - D(1 - A_{31}/\gamma_1)/\gamma_3) - 2|V_p|^2(A\Gamma_{13} - B(1 - A_{32}/\gamma_2)/\gamma_3) - 4|V_p|^2|V_D|^2(AC - BD)[\Gamma_{13}\Gamma_{23} - (1 - A_{32}/\gamma_2) \times (1 - A_{31}/\gamma_1)/(\gamma_3\gamma_3)].$$

The absorption cross sections are related to the transition dipole moments by

$$\sigma_p = k_p|p_{13}|^2/(\epsilon_0\hbar\gamma_{13}), \qquad \sigma_D = k_D|p_{23}|^2/(\epsilon_0\hbar\gamma_{23}).$$

Small-Signal Gain

The small-signal gain is obtained for $|V_D| = 0$. This leads to

$$\alpha_p{}^v = \sigma_p\delta_{13}{}^p(v)\rho_{11}{}^0/(1 + P), \quad \text{(A5)}$$

with

$$P = I_p/I_p{}^0 = 2\Gamma_{13}V_p{}^2/\gamma_{13}$$

and

$$\delta_{13}{}^p(v) = [1 + (\Omega_p - k_pv)^2/[\gamma_{13}{}^2(1 + P)]]^{-1}, \quad \text{(A6)}$$

where

$$I_p = \epsilon_0c\mathbf{E}_p{}^2/2, \qquad I_p{}^0 = \hbar^2\epsilon_0c\gamma_{13}/(|p_{13}|^2\Gamma_{13})$$

have been used.

Here $\delta_{13}{}^p(v)$ is a power-broadened Lorentzian line shape. The small-signal gain coefficient for the dimer laser is given by Eq. (13).

The normalized line-shape functions $E(v)$ and $G(v)$ are defined as

$$E(v) = \mathrm{Im}[-\Delta_{12}{}^*\gamma_{23}/(\Delta_{12}{}^*\Delta_{23} + |V_p|^2)], \quad \text{(A7)}$$

$$G(v) = \delta_{13}{}^p\,\mathrm{Im}[\Delta_{13}\gamma_{23}/(\Delta_{12}{}^*\Delta_{23} + |V_p|^2)]. \quad \text{(A8)}$$

Low-Pump-Power Limit

For low-pump intensities I_p such that $P \ll 1$, the Eqs. (A6) and (A8) can be expanded in a power series in P. Retaining only terms proportional to P gives the gain coefficients in the small-signal, low-pump limit:

$$\alpha_P{}^v = \sigma_P\rho_{11}{}^0P\delta_{13}(v), \quad \text{(A9)}$$

$$\alpha_D{}^v = \sigma_D\rho_{22}{}^0\delta_{23}(v) - \sigma_D\rho_{11}{}^0(1 - A_{32}/\gamma_2)\gamma_1/(\gamma_1 + \gamma_3)P\delta_{13}(v)\delta_{23}(v) - \sigma_D\rho_{11}{}^0/(2\gamma_{13}\Gamma_{13})P\,\mathrm{Im}[\gamma_{23}\gamma_{13}{}^2/(\Delta_{12}{}^*\Delta_{23}\Delta_{13}{}^*)] - \sigma_D\rho_{22}{}^0\gamma_{13}/(2\gamma_{23}{}^2\Gamma_{13})P\,\mathrm{Im}[\gamma_{23}{}^3/(\Delta_{12}{}^*\Delta_{23}\Delta_{23})]. \quad \text{(A10)}$$

In this limit, the line-shape functions $\delta_{ij}(v)$, with

$$\delta_{13} = (1 + (\Omega_p - k_pv)^2/\gamma_{13}{}^2)^{-1},$$

$$\delta_{23} = (1 + (\Omega_D - \epsilon k_Dv)^2/\gamma_{23}{}^2)^{-1},$$

are independent of P.

ACKNOWLEDGMENTS

We greatly appreciate the expert technical assistance of Lothar Meyer. This research has been supported by the Deutsche Forschungsgemeinschaft through SFB 91, "Energy transfer in atomic and molecular collisions."

* Permanent address, Laser Optronics GmbH, Hertzstrasse 6, D-8047 Munich, Federal Republic of Germany.

† Permanent address, Université d'Abidjan, 04-B.P. 322, Abidjan 04 04, Cote d'Ivoire.

‡ Permanent address, Spectra Technology, Inc., Bellevue, Washington 98004.

REFERENCES

1. F. P. Schäfer, ed., *Dye Lasers*, Vol. 1 of Topics in Applied Physics (Springer-Verlag, New York, 1977).
2. L. F. Mollenhauer, "Color center laser" in *Laser Handbook*, M. L. Stitch and R. Bass, eds. (North-Holland, Amsterdam, 1985), Vol. 4, pp. 143–228.
3. B. Wellegehausen, "Optically pumped cw dimer lasers," IEEE J. Quantum Electron. **QE-15,** 1108–1130 (1979).
4. J. C. White, "Stimulated Raman Scattering," in *Tunable Lasers*, L. F. Mollenauer and J. C. White, eds., Vol. 59 of Topics in Applied Physics (Springer-Verlag, Heidelberg, 1987), pp. 115–207.
5. Ch. Salomon, D. Hils, and J. L. Hall, "Laser stabilization at the millihertz level" J. Opt. Soc. Am. B **5,** 1576–1587 (1988).
6. M. Becker, U. Gaubatz, K. Bergmann, and P. L. Jones, "Efficient and selective population of high vibrational levels by stimulated near resonance Raman scattering," J. Chem. Phys. **87,** 5064–5076 (1987).
7. U. Hefter, J. Eichert, and K. Bergmann, "An optically pumped supersonic iodine beam laser," Opt. Commun. **52,** 330–335 (1985).
8. J. B. Koffend, F. J. Wodarczyk, R. Bacis, and R. W. Field, "Collisional relaxation of highly excited vibrational levels of the I_2 $X\,^1\Sigma_g^+$ state using an I_2 optically pumped laser," J. Chem. Phys. **72,** 478–483 (1980).
9. S. J. Davis, "Continuous wave optically pumped iodine monofluoride $B\,^3\Pi_0 \rightarrow X\,^1\Sigma$ laser" J. Chem. Phys. **82,** 4831–4837 (1985).
10. C. N. Man-Pichot and A. Brillet, "Precise measurement and assignment of cw laser emission lines from optically pumped Na_2 and Li_2 molecules," IEEE J. Quantum Electron. **QE-16,** 1103–1108 (1980).
11. M. A. Henesian, R. L. Herbst, and R. L. Byer, "Optically pumped superfluorescent Na_2 molecular laser," J. Appl. Phys. **47,** 1515–1518 (1976).
12. B. Wellegehausen, S. Shahdin, D. Friede, and H. Welling, "Continuous laser oscillation in diatomic molecular sodium," Appl. Phys. **13,** 97–99 (1977).
13. S. Shahdin, B. Wellegehausen, and J. G. Ma, "Ultra-violet excited laser emission in Na_2," Appl. Phys. B **29,** 195–200 (1982); J. T. Bahns, K. K. Verma, A. R. Rajaei-Rizi, and W. C. Stwalley, "Optically pumped ring laser oscillation to vibrational levels near dissociation and to the continuum in Na_2," Appl. Phys. Lett. **42,** 331–338 (1983).
14. P. L. Jones, U. Gaubatz, U. Hefter, K. Bergmann, and B. Wellegehausen, "Optically pumped sodium-dimer supersonic-beam laser," Appl. Phys. Lett. **42,** 222–224 (1983).
15. S. R. Leone and K. G. Kosnik, "A tunable visible and ultraviolet laser on S_2," Appl. Phys. Lett. **30,** 346–348 (1977).
16. B. Wellegehausen, A. Topouzkhanian, C. Effantin, and J. d'Incan, "Optically pumped continuous multiline Se_2-laser," Opt. Commun. **41,** 437–442 (1982).
17. B. Wellegehausen, D. Friede, and G. Steger, "Optically pumped continuous Bi_2 and Te_2 lasers," Opt. Commun. **26,** 391–395 (1978).
18. F. J. Wodarczyk and H. R. Schlossberg, "An optically pumped molecular bromine laser," J. Chem. Phys., **67,** 4476–4482 (1977).
19. S. Drosch and G. Gerber, "Optically pumped cw molecular bismuth laser," J. Chem. Phys. **77,** 123–130 (1982).
20. R. L. Byer, R. L. Herbst, H. Kildal, and M. D. Levenson, "Optically pumped molecular iodine vapor-phase laser," Appl. Phys. Lett. **20,** 463–466 (1972).
21. B. Wellegehausen, K. H. Stephan, D. Friede, and H. Welling, "Optically pumped continuous I_2 molecular laser," Opt. Commun. **23,** 157–161, 1977; J. B. Koffend, R. Bacis, and R. W. Field, "Continuous wave optically pumped iodine laser," J. Mol. Spectrosc. **77,** 202–212 (1979).
22. B. Wellegehausen and H. H. Heitmann, "Experiments on optically pumped three-level dimer lasers," Appl. Phys. Lett. **34,** 44–47 (1979).
23. B. Wellegehausen, W. Luhs, H. Welling, and A. Topouzkhanian, "New developments in optically pumped dimer lasers," Appl. Phys. B **28,** 195–196 (1982); W. Luhs and B. Wellegehausen, "Raman tuning of optically pumped continuous dimer lasers," Opt. Commun. **46,** 121–125 (1983).
24. R. J. DeYoung, "Low threshold solar pumped iodine laser," IEEE J. Quantum Electron. **QE-22,** 1019–1023 (1986).
25. J. V. Moloney, J. S. Uppal, and R. G. Harrison, "Origin of chaotic relaxation oscillations in an optically pumped molecular laser," Phys. Rev. Lett. **59,** 2868–2871 (1987); S. C. Mahendale and R. G. Harrison, "Theoretical analysis of instabilities in optically pumped molecular lasers," Opt. Commun. **60,** 257–269 (1986).
26. T. Q. Wu and C. O. Weiss, "Chaotic emission of a molecular electronic transition laser," Opt. Commun. **61,** 337–338 (1987).
27. J. B. Anderson, in *Molecular Beams and Low Density Gas Dynamics*, P. P. Wegener, ed. (Dekker, New York, 1974), pp. 1–91.
28. D. Miller, in *Atomic and Molecular Beam Methods*, G. Scoles, ed. (Oxford U. Press, Oxford, 1988).
29. U. Gaubatz, "Untersuchungen an einem optisch gepumpten Na_2-Düsenstrahllaser," *Diplom* dissertation (University of Kaiserslautern, Kaiserslautern, Federal Republic of Germany, June 1983).
30. H. Ashkenas and F. S. Sherman, "The structure and utilisation of supersonic free jets in low density wind tunnels," in *Proceedings of the Fourth International Symposium on Rarefied Gasdynamics*, J. H. de Leeuw, ed. (Academic, New York, 1966), Vol. II, pp. 84–105.
31. H. C. W. Beijerinck and N. F. Verster, "Absolute intensities and perpendicular temperatures of supersonic beams of polyatomic gases," Physica **111C,** 327–352 (1981); H. C. W. Beijerinck, G. H. Kaashoek, J. P. M. Beijers, and M. J. Verheyen, "Non-Maxwellian velocity distributions in the transition region of supersonic expansions of the noble gases He, Ne and Ar," Physica **121C,** 425–436 (1983).
32. A. E. Beylich, "Struktur von Überschall-Freistrahlen aus Schlitzblenden," Z. Flugwiss. Weltraumforsch. **3,** 48–57 (1979).
33. M. Sulkes, C. Jouvet, and S. A. Rice, "Theoretical and experimental characterization of supersonic expansions from slit sources," Chem. Phys. Lett. **87,** 515–519 (1982).
34. K. Bergmann, U. Hefter, and P. Hering, "Molecular beam diagnostics with internal state selection: velocity distribution and dimer formation in a supersonic Na/Na_2 beam," Chem. Phys. **32,** 329–348 (1978).
35. F. Aerts, H. Hulsman, and P. Willems, "Laser induced fluorescence study of the first part of a Na/Na_2 free jet expansion: dimer formation and excitation-energy transfer," Chem. Phys. **68,** 233–249 (1982).
36. R. Engelhardt, Th. Lorenz, K. Bergmann, Th. Mietzner, and A. Palczewski, "Shape analysis of the velocity distribution in supersonic Ar beams: comparison between experiment and theory," Chem. Phys. **95,** 417–433 (1985).
37. P. Hering, "Laserspektroskopische Untersuchung eines Na/Na_2 Überschallstrahles mit interner Zustandsselektion," Ph. D. dissertation (University of Kaiserslautern, Kaiserlautern, Federal Republic of Germany, 1978).
38. M. L. Janson and J. P. Klavins, "Effective cross sections of excitation transfer from separate $v'J'$ states of Na_2 ($B\,^1\Pi_0$) to atomic levels of Na and K," Chem. Phys. Lett. **86,** 453–452 (1982).
39. A. Yariv, *Quantum Electronics* (Wiley, New York, 1975).
40. M. Sargent, M. Scully, and W. Lamb, *Laser Physics* (Addison-Wesley, Reading, Mass., 1974).
41. V. S. Letokhov and V. P. Chebotayev, *Nonlinear Spectroscopy*, Springer Series in Optical Science (Springer-Verlag, Berlin, 1977).
42. K. Blum, "Density matrix formalism and applications in spectroscopy," in *Progress in Atomic Spectroscopy*, W. Hanle and H. Kleinpoppen, eds. (Plenum, New York, 1978), pp. 71–110.
43. T. Hänsch and P. Toschek, "Theory of a three-level gas laser amplifier," Z. Phys. **236,** 213–244 (1970).
44. M. D. Levenson, *Introduction to Nonlinear Laser Spectroscopy* (Academic, New York, 1982), p. 33.
45. L. Allan and J. H. Eberly, *Optical Resonances and Two-Level Atoms* (Wiley, New York, 1975), p. 29.
46. A. Yariv, *Quantum Electronics* (Wiley, New York, 1975), p. 176.
47. U. Gaubatz, M. Becker, and K. Bergmann, "Vibrational level

dependence of Na_2–Ne scattering cross sections at very low collision energy," J. Chem. Phys. **89,** 2583–2584 (1988).
48. M. Lewenstein and K. Rzazewski, "Noise reduction in a Raman-ring driven by a chaotic pump," Opt. Commun. **63,** 174–177 (1987); J. R. Kuklinski and K. Rzazewski, "Raman scattering in a ring-cavity linear regime," J. Opt. Soc. Am. B **5,** 53–60 (1988); J. R. Kuklinski, "Raman scattering: fluctuations, ring cavity and self-pulsing," Ph.D. dissertation (Institute of Theoretical Physics of the Polish Academy of Sciences, Warsaw, 1988).
49. D. R. Jones and D. C. Laine, "Step-tunable iodine molecular beam laser in the visible," presented at the European Conference on Quantum Electronics, Hannover, 1988.
50. R. Möller, "Photofragmentspektroskopie an Na_2," Ph.D. dissertation (University of Freiburg, Freiburg, Federal Republic of Germany, 1985); G. Gerber and R. Möller, "Optical–optical double-resonance spectroscopy of high vibrational levels of the Na_2 $A\,^1\Sigma_u^+$ -state in a molecular beam," Chem. Phys. Lett. **113,** 546–53 (1985); W. T. Zemke, K. K. Verma, T. Vu, and W. C. Stwalley, "An investigation of radiative transition probabilities of the $A\,^1\Sigma_g^+$–$X\,^1\Sigma_g^+$ bands of Na_2," J. Mol. Spectrosc. **85,** 150–76 (1981); P. Kusch and M. M. Hessel, "Analysis of the $B\,^1\Pi_u$–$X\,^1\Sigma_g^+$ band system of Na_2," J. Chem. Phys. **68,** 2591–606 (1978); W. J. Stevens, M. M. Hessel, B. J. Bertoncini, and A. C. Wahl, "Theoretical transition dipole moments and lifetimes for the $A\,^1\Sigma_u^+$–$X\,^1\Sigma_g^+$ system of Na_2," J. Chem. Phys. **66,** 1477–82 (1977); W. Demtröder, W. Stetzenbach, M. Stock, and J. Witt, "Lifetimes and Franck–Condon factors for the $B\,^1\Pi_u$–$X\,^1\Sigma_g^+$ system of Na_2," J. Mol. Spectrosc. **61,** 382–94 (1976).